IEEE Access
Multidisciplinary | Rapid Review | Open Access Journal

Received April 16, 2018, accepted May 13, 2018, date of publication May 16, 2018, date of current version June 19, 2018.

Digital Object Identifier 10.1109/ACCESS.2018.2837156

State of Charge Estimation for Lithium-Ion Battery Using Recurrent NARX Neural Network Model Based Lighting Search Algorithm

MOLLA S. HOSSAIN LIPU[1,2], (Student Member, IEEE), MAHAMMAD A. HANNAN[3], (Senior Member, IEEE), AINI HUSSAIN[1], (Member, IEEE), MOHAMAD H. M. SAAD[1], AFIDA AYOB[1], AND FREDE BLAABJERG[4], (Fellow, IEEE)

[1]Center for Integrated Systems Engineering and Advanced Technologies (INTEGRA), Faculty of Engineering and Built Environment, Universiti Kebangsaan Malaysia, Bangi 43600, Malaysia
[2]Department of Electrical and Electronic Engineering, University of Asia Pacific, Dhaka 1209, Bangladesh
[3]Department of Electrical Power Engineering, Universiti Tenaga Nasional, Kajang 43000, Malaysia
[4]Department of Energy Technology, Alborg University, 9100 Aalborg, Denmark

Corresponding author: Mahammad A. Hannan (hannan@uniten.edu.my)

This work was supported in part by the Ministry of Higher Education, Malaysia, and in part by Universiti Kebangsaan Malaysia under Grants FRGS/1/2017/TK04/UKM/02/12 and DIP-2015-012.

ABSTRACT State of charge (SOC) is one of the crucial parameters in a lithium-ion battery. The accurate estimation of SOC guarantees the safe and efficient operation of a specific application. However, SOC estimation with high accuracy is a serious concern to the automobile engineer due to the battery nonlinear characteristics and complex electrochemical reactions. This paper presents an improved nonlinear autoregressive with exogenous input (NARX)-based neural network (NARXNN) algorithm for an accurate and robust SOC estimation of lithium-ion battery which is effective and computationally rich for controlling dynamic system and predicting time series. However, the accuracy of recurrent NARXNN depends on the amount of input order, output order, and hidden layer neurons. The unique contribution of the improved recurrent NARXNN-based SOC estimation is developed using lighting search algorithm (LSA) for finding the best value of input delays, feedback delays, and hidden layer neurons. The contributions are summarized as: 1) the computational capability of NARXNN model which does not require battery model and parameters rather only needs current, voltage, and temperature sensors; 2) the effectiveness of LSA which is verified with particle swarm optimization; 3) the adaptability, efficiency, and robustness of the model which are evaluated using FUDS and US06 drive cycles at varying temperatures conditions; and 4) the performance of the proposed model which is compared with back propagation neural network and radial basis function neural network optimized by LSA using different error statistical terms and computational time. Furthermore, a comparative analysis of SOC estimation in proposed method and existing techniques is presented for validation of NARXNN performance. The results prove that the proposed NARXNN model achieves higher accuracy with less computational time than other existing SOC algorithms under different temperature conditions and electric vehicle drive cycles.

INDEX TERMS State of charge, lithium-ion battery, NARX neural network, lighting search algorithm.

I. INTRODUCTION

Global emissions have been one of the alarming issues in recent decades. Transportation contributes 14% of global emissions which is mainly caused by gasoline and diesel based vehicles [1]. To address the challenges, electric vehicle (EV) has been considered as one of the promising alternatives which use the sustainable energy resources to reduce greenhouse gas emissions and global warming effect. The performance and efficiency of EV have been enhanced substantially in recent years due to the high storage capacity and long lifespan of energy storage devices. Nevertheless, the development of EVs with improved quality, efficient energy storage management system is a serious concern to the researcher and vehicle manufacturer [2]. There are different

kinds of energy storage devices that are being actively employed in vehicle operation. Among them, lithium-ion battery is extensively used in EV application due to high efficiency, high energy density, long lifespan, no memory effect, low hysteresis, and environmental friendliness [3].

State of charge (SOC) is a vital indicator which signifies the remaining charge left inside a lithium-ion battery to drive a vehicle [4]. However, an accurate SOC estimation is a big challenge due to the complex electrochemical reaction of the lithium-ion battery. In addition, lithium-ion battery is very sensitive to aging and temperature [5]. In order to achieve a stable and reliable operation of EV, SOC estimation with high accuracy is compulsory. An accurate and robust SOC estimation technique will avoid overcharge, over discharge and overheating which will increase the lifecycle of batteries [6]. SOC is estimated based on current integration which is estimated using the available current capacity divided by the nominal capacity [7] as presented in (1),

$$SOC = SOC_0 - \frac{1}{C_n}\int i\eta dt \tag{1}$$

where SOC_0 represents the initial value of SOC, i is the battery current, C_n is the nominal capacity; t is time and η is the columbic efficiency.

Several methods on SOC estimation have been introduced in recent years. Coulomb counting method is a straightforward approach and easy to apply in battery management system (BMS) with low power consumption [8]. However, the method fails to determine the initial value of SOC accurately which results in the cumulative effect. Open circuit voltage (OCV) estimates SOC offline with high accuracy [9]. However, OCV requires long rest time to reach stable condition and cannot operate online. Kalman filter (KF) method has been used extensively for SOC estimation [10]. Nevertheless, KF provides unsatisfactory results due to temperature variation, inappropriate battery model, and highly nonlinear characteristics of battery system. A particle filter (PF) estimates SOC with high accuracy and less execution time [11]. However, PF requires complex computation tool to solve the problem. H∞ Filter is demonstrated to be a better model than KF in terms of high accuracy and less computational cost [12]. Nonetheless, the method does not provide a strong robustness due to hysteresis, and temperature variations. The nonlinear observer [13] and sliding mode observer [14] have enhanced robustness in terms of convergence speed and high precision against the model uncertainty and disturbances. However, the methods could provide inaccurate results if the controller is not designed appropriately. An intelligent approach called fuzzy logic can estimate SOC with temperature variation, and noises [15]. Nonetheless, the fuzzy method requires a large storage device for keeping a huge amount of training data. Support vector machine (SVM) obtains satisfactory performance in estimating SOC quickly and accurately in a nonlinear battery model [16]. However, highly complex computation makes the process difficult to be executed in the BMS system.

To address the above challenges, an improved artificial neural network (ANN) model is proposed with optimal parameters under dynamic load profiles and different temperatures. ANN is well suited for modelling complex and time-varying systems and will not depend on battery model and mathematical relationship [17]. Nevertheless, ANN algorithm has computation complexity such as slow convergence, data over-fitting and can easily be trapped into local minima. However, the computational complexity of ANN can be reduced by choosing the appropriate training algorithm, activation function, number of hidden layers, number of neurons, learning rate, spread value, input and output orders. The ANN methods have already been introduced for SOC estimation including back-propagation neural network (BPNN) [18], [19], radial basis function neural network (RBFNN) [20], [21], recurrent neural network (RNN) [22]. However, the existing ANN methods have used time-consuming trial and error approach for finding the correct value of parameters that are inefficient and do not provide an optimal solution.

This paper develops an improved RNN with an optimization algorithm to enhance the estimation intelligence and robustness of SOC estimation. Nonlinear autoregressive with exogenous inputs (NARX) model of RNN is ideal for battery energy storage systems since NARX is suitable for predicting complex and nonlinear system. The optimization technique is significant in SOC estimation for obtaining the best values in battery models under different conditions. Recently, heuristic optimization techniques are extensively utilized to solve problems. These techniques are stochastic algorithms that mimic the processes of natural phenomena, such as self-organization, natural evolution, and natural selection. Lighting Search Algorithm (LSA) is superior to other algorithms in terms of fast convergences speed and reduction of error. LSA uses fast particles known as projectiles to search for the optimal solution using the concept of the natural lightning phenomenon. In [23], the efficiency and reliability of LSA are evaluated using 24 benchmark functions with different characteristics.

In this research, the accuracy of SOC estimation is improved with LSA by finding the appropriate value of input delays, feedback delays and hidden neurons in NARXNN model. The proposed model performance is evaluated with PSO technique as well as other neural network approaches under different discharge profiles and temperatures impacts. The NARXNN based LSA model features high accuracy, high convergence speed, and strong robustness without depending any battery model and mathematical relationship. The developed model might have good prospects to be applied in a wide number of lithium-ion battery storage systems in EV and sustainable energy applications. The paper is structured as follows. Section two and three narrate the NARXNN architecture and LSA execution, respectively. The method of model development is depicted in section four. Section five illustrates results and discussion. Section six presents the conclusion.

II. RECURRENT NARX NEURAL NETWORK MODEL

Recurrent neural network (RNN) is supervised machine learning method, with one or more feedback loops. In [24], RNN is designed based on control methods for the accurate and robust solution of the algebraic equation with time-varying parameters. NARX is a subclass of RNN which is appropriate for predicting non-linear and time series problems. NARXNN network uses limited feedbacks form the output layers instead of hidden layers. NARXNN performs better than the conventional RNNs in terms of learning capability, convergence speed, generalization performance and high accuracy [25]. The mathematical expression of NARXNN can be written as,

$$y(n+1) = f\left[y(n), \ldots, y\left(n-d_y\right); u(n), \ldots, u\left(n-d_u\right)\right] \quad (2)$$

where $u(n)$ and y (n) represent the input and output of the NARXNN model, respectively at discrete time step n. d_u and d_y represent input delay and output delay, respectively. The function f (.) is a nonlinear function that can be approximated by multilayer perceptron (MLP) [26]. The general NARXNN architecture is indicated in Fig. 1. NARXNN model with one-time series can be represented as

$$y(n+1) = f_0\left[b_0 + \sum_{h=1}^{Nh} w_{ho} f_h\left(b_h + \sum_{i=0}^{d_u} w_{ih} u(n-i) + \sum_{j=0}^{d_y} w_{jh} y(n-j)\right)\right] \quad (3)$$

where w_{ih} w_{ho} and w_{jh} denote the weights from the input layer to the hidden layer, hidden layer to output layer and output feedback layer to the hidden layer respectively. b_0 and b_h are the biases. f_h (.) and f_0 (.) are functions of the hidden layer and output layer, respectively [26]. A tangent sigmoid transfer function (tansig) and a linear transfer function (purelin) are used for the perceptron at the hidden layer and output layer, respectively [27].

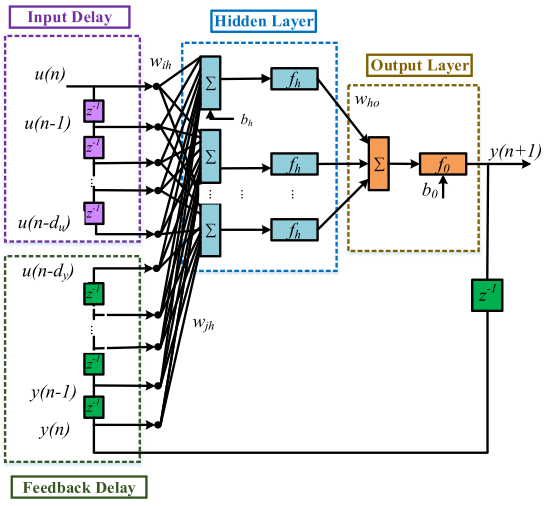

FIGURE 1. Recurrent NARXNN architecture.

NARXNN can be employed in multiple inputs and multiple outputs time series applications. Since this research considers current, voltage and temperature as inputs and SOC as output, therefore the general NARXNN with three inputs and one output can be mathematically expressed as, (4) as shown at the top of the next page, where w_{i1h}, w_{i2h} and w_{i3h} are the weights between the first input to the hidden neurons, between the second input to the hidden neurons and between the third input to the hidden neurons, respectively [26].

III. LIGHTING SEARCH ALGORITHM

Shareef *et al.* [23] invented an advanced metaheuristic optimization algorithm called LSA in 2005. The natural occurrence of lighting concept is used for the development of LSA. The searching procedures of LSA for achieving optimal solutions is based on the technique of step leader propagation. The particles of LSA is known as projectiles which are similar to ''swarm'' or ''particle'' term used in other optimization methods. The projectiles characterize the initial population and are arranged in a binary tree structure. The projectiles could also be organized in the synchronous form of two leaders at fork points rather than using the conventional technique of step leader.

A. PROPERTIES OF THE PROJECTILES

There is a loss of kinetic energy when a projectile travels in the atmosphere and then have a collision with other atoms and molecules. The mathematical expressions of the kinetic energy E_p and velocity of a projectile v_p are presented by,

$$E_p = \left(\left(\frac{1}{\sqrt{1-\left(\frac{v_p}{c}\right)^2}}\right) - 1\right) mc^2 \quad (5)$$

$$v_p = \left[1 - \left(\frac{1}{\sqrt{1-\left(\frac{v_0}{c}\right)^2}} - \frac{sF_i}{mc^2}\right)^{-2}\right]^{-\frac{1}{2}} \quad (6)$$

where v_p and v_0 represent current velocity and initial velocity of the projectile, respectively, F_i is the ionization constant rate, c is the light speed, m is the projectile mass and s is the path length that a projectile travels.

It is clearly evident from the above two equations that projectile kinetic energy and velocity are strongly dependent on the mass of projectile and position of leader tip. When the projectile needs to travel a long way with low mass, the projectile will not have enough energy to ionize or explore a long distance. In that situation, the projectile can only travel to nearby distance for ionizing or exploitation. Therefore, the exploration and exploitation capabilities of the LSA are controlled by the relative energies of the step leaders.

B. PROJECTILES MODELLING AND STEP LEADER MOVEMENT

There are three categories of projectiles that are established in LSA including transition projectiles, space projectiles, and lead projectile. Transition projectiles generate the first step

$$y(n+1) = f_0\left[b_0 + \sum_{h=1}^{N} w_{ho} \cdot f_h\left(b_h + \sum_{i1=0}^{d_{u1}} w_{i1h}u_1(n-i1) + \sum_{i2=0}^{d_{u2}} w_{i2h}u_2(n-i2) + \sum_{i3=0}^{d_{u3}} w_{i3h}u_3(n-i3) + \sum_{j=0}^{d_y} w_{jh}y(n-j)\right)\right] \quad (4)$$

leader population N, the space projectiles try to become the leader and the lead projectile represents the located projectile which is initiated by N population number of step leader.

1) TRANSITION PROJECTILE

A leader tip is generated in a random order at the initial phase due to the formation of the ejected projectile from the thunder cell. The random number could be modeled as probability density function $f(x^T)$ that represents the solution space on the open interval. The probability density function $f(x^T)$ of the standard uniform distribution can be written as,

$$f\left(x^T\right) = \begin{cases} \dfrac{1}{b-a} & for\ a \le x^T \le b \\ 0 & for\ x < a\ or\ x^T > b \end{cases} \quad (7)$$

where x^T is a random value that may deliver a result of the initial tip energy E_{sl_i} of the step leader sl_i, a and b represent the lower and upper bounds, respectively, of the solution space, $SL = [sl_1, sl_2, sl_3, ..., sl_N]$ represent the step leader population of N, $P^T = \left[p_1^T, p_2^T, p_3^T \ldots \ldots \ldots \ldots, p_N^T\right]$ represent solution dimensions that are needed for the population.

2) SPACE PROJECTILE

The leaders need to travel in the space using the active projectiles by segment ionization in the surrounding area of the old leader tip in the next step, after the N step leader tips advance. A partial random number model can be designed in the form of exponential distribution with shaping parameter, μ and the position of the space projectile, $P^S = \left[p_1^S, p_2^S, p_3^S \ldots \ldots \ldots \ldots, p_N^S\right]$ at $step + 1$. The probability density function $f\left(x^S\right)$ of an exponential distribution is expressed as,

$$f\left(x^S\right) = \begin{cases} \dfrac{1}{\mu} e^{\frac{-x^S}{\mu}} & for\ x^S \ge 0 \\ 0 & for\ x^S \le 0 \end{cases} \quad (8)$$

It is observed form (8) that shaping parameter μ controls the position and direction of space projectile. In the LSA, μ_i outlines a specific space projectile, p_i^S states the distance between the lead projectile, p^L and the space projectile, p_i^S. The revised position of p_i^S at $step + 1$ is represented by,

$$p_{i\_new}^S = p_i^S \pm exprand\ (\mu_i) \quad (9)$$

where exprand represents the exponential random number. Nevertheless, the updated location does not provide confirmation of the formation of a stepped leader propagation or channel until the capacity of the projectile, $E_{p\_i}^S$ is higher than the energy of step leader, E_{sl_i} to expand the channel or until a satisfactory result is achieved. If $p_{i\_new}^S$ obtains a satisfactory result at $step+1$, then the corresponding stepped leaders, sl_i spread out to a new position, sl_{i_new}, and p_i^S is upgraded to $p_{i\_new}^S$. Else, they keep unmoved until the next step is reached. If $p_{i\_new}^S$ expands beyond sl_{i_new}, the most expanded leader turns into the lead projectile.

3) LEAD PROJECTILE

The step leader and the projectile do not have sufficient potential for ionization in large extent when they explore closest to the earth. Thus, a random number model can be developed using the lead projectile generated by the standard normal distribution with the shape parameter, μ, and the scale parameter, σ. The normal probability density function $f(x^L)$ is demonstrated by the following equation.

$$f(x^L) = \frac{1}{\sigma\sqrt{2\pi}} e^{\frac{-(x^L-\mu)^2}{2\sigma^2}} \quad (10)$$

It is seen from (10) that shape parameter confirms the searching capability of the lead projectile in all directions whereas scale parameter confirms the exploitation ability. The scale parameter exponentially declines as it advances toward the ground or as it attains the optimal solution. The updated position of p^L at $step + 1$ can be expressed by,

$$p_{i\_new}^L = P_i^L + normrand(\mu_L, \sigma_L) \quad (11)$$

where, normand is a random number developed by a normal distribution function. Likewise, if $p_{i\_new}^L$ obtains a reasonable solution at $step + 1$, and $E_{p\_i}^L > E_{sl\_i}$ then p_i^L is revised to $p_{i\_new}^L$. Otherwise, they keep unchanged until the next step is attained.

C. FORKING PROCEDURE

Forking is another vital property of stepped leader during which the number of projectile and the population size are increased through channels formation. In LSA, forking is occurred in two methods. The first method is the development of the symmetrical channels due to the nuclei collision of the projectile by the opposite number,

$$\overline{p}_i = a + b - p_i \quad (12)$$

where $\overline{p_i}$ and p_i represents the opposite and original projectiles in one-dimension, respectively, and a and b denote the boundary limits. The forking leader chooses the appropriate fitness value of $\overline{p_i}$ and p_i to improve some complex solutions in population.

In the second method of forking, a channel is expected to come out at a successful step leader tip since the most unsuccessful leader redistributes energy after numerous propagation tests. The redistribution of the unsuccessful leader can be achieved by assigning the maximum permissible trial

numbers as channel time. This approach does not increase the size of the step leaders' population.

IV. RECURRENT NARXNN BASED LSA MODEL

At First, the estimation of SOC begins by collecting data from FUDS and US06 drive cycles. Three basic input variables are chosen namely current, voltage and temperatures. Then, data is pre-processed and normalized. In this research, 5 consecutive FUDS cycles and 12 cycles consecutive US06 cycles have been selected for discharging battery as well as for training and testing. The duration of one FUDS and US06 cycle is 1372 seconds and 600 seconds respectively. Later, the entire FUDS and US06 cycles are split into two data sets. The model training is performed using 70% selected data and testing is executed using 30 % selected data. The Levenberg-Marquardt (LM) algorithm is used for model training due to its high speed and accuracy [28]. In this study, the maximum number of epochs is 1000 and the performance goal is set as 0.00001. After that, the input delays, feedback delays, and hidden neurons are optimized with LSA based on the lowest value of an objective function using (13),

$$Objective\ Function = min\left[\frac{1}{N}\sum_{i=1}^{N}(I_{es}-I_a)^2\right] \quad (13)$$

where I_{es} represents the estimated value, I_a is actual value and N is a number of observations.

LSA optimization improves the performance efficiency of the NARXNN with less variance, less error and best fitting for the prediction function while avoiding under-fitting and over-fitting problem. Finally, the optimal parameters proceed to recurrent NARXNN for training and testing using tansig activation function and LM training algorithm. The schematic diagram of the recurrent NARXNN based LSA model is shown in Fig. 2.

A. DATA PREPARATION

A test battery called 18650 lithium nickel manganese cobalt oxide ($LiNiMnCoO_2$ or NMC) was used in this research which has a nominal capacity and voltage of 2.0 Ah and 3.6 V, respectively. NMC has lower and upper cut-off voltage of 2.5 V and 4.2 V, respectively. Charging of lithium-ion battery was performed based on constant current-constant voltage (CCCV) approach. The measurements were recorded in a 1-second interval. Two drive cycles, namely FUDS [29] US06 [30] were used for data training and testing. A battery test bench was developed [31] to collect battery data which included NMC battery, a host computer to monitor and control data, battery cycler (Arbin BT2000) to control battery charging and discharging, a thermal chamber to measure cell temperature. SOC estimation is based on NARXNN model with three influential factors including current, voltage and temperature. Data were collected at low temperature (0°C), medium temperature (25°C), and high temperature (45°C). An appropriate data normalization can make the training process of NARXNN more efficient and robust. Furthermore, data normalization can remove the negative effect that

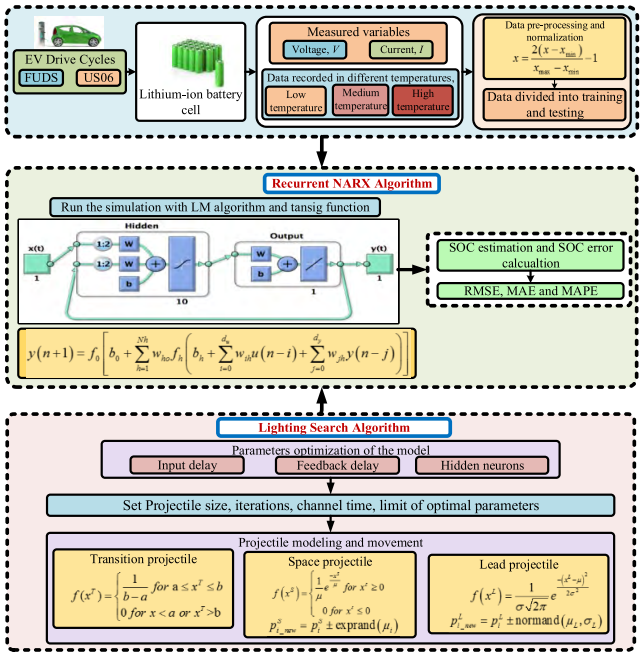

FIGURE 2. Schematic diagram of recurrent NARXNN based LSA model for SOC estimation.

improves the convergence rate. In this study, input data are normalized to a range [−1,1] as shown in (14).

$$x = \frac{2\,(x - x_{min})}{x_{max} - x_{min}} - 1 \quad (14)$$

where $x_{\max}$ and $x_{\min}$ are the maximum and minimum value of input vector x of the NARXNN model. The validation dataset is scaled using the same range used in the training data. The input variables of FUDS and US06 drive cycle are shown in Fig. 3 in Fig. 4, respectively.

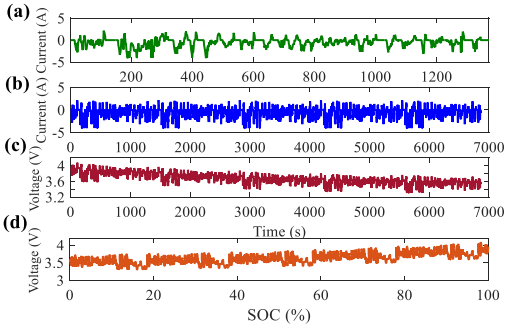

FIGURE 3. FUDS drive cycle (a) current in one cycle (b) current (c) voltage (c) voltage against SOC.

B. LSA IMPLEMENTATION

The aim of LSA is to achieve the best solution by reducing the objective function using the input data and constraints through an iterative procedure. The procedures of LSA are summarized as follows.

i. At first, LSA algorithm starts with declaring parameter values including population size, number of iterations

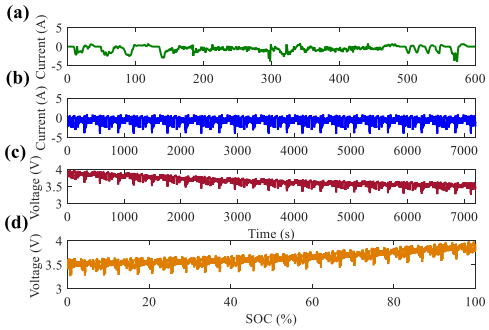

FIGURE 4. US06 drive cycle (a) current in one cycle (b) current (c) voltage (c) voltage against SOC.

and channel time. In this study, the swarm size is 50 and iteration number is 100. Also, the maximum number of channel time is considered to be 10. In addition, the boundary of three dimensions; input delays, feedback delays, and hidden layer neurons is assigned. For input delays and feedback delays, the limit is set between '1' and '10' and for hidden nodes, the limit lies between '0' and '20'.

ii. The step leaders of input delays, feedback delays, and hidden layer neurons are generated randomly within the boundary range.

iii. The NARXNN training process is executed based on LM algorithm and tansig function. Then, the objective function of each step leader is calculated.

iv. The iteration method initiates to search for the best objective function among all the step leaders.

v. The channel time is reset by eliminating bad channel through the movement of step leader from worst to best.

vi. The best or worst step leaders are estimated.

vii. The kinetic energy (*Ep*) is revised and the NARXNN activation function is executed again for training and the objective function is reassessed for step leader.

viii. Space and lead particles are ejected.

ix. The position and direction of space and lead projectiles are upgraded if the energy of the projectile is higher than the energy of step leader using (9) and (11).

x. The updated projectile for input delays, feedback delays, and hidden layer neurons are re-initialized within the boundary limit. The NARXNN training is performed again and the objective function is re-assessed for space and lead particles.

xi. The occurrence of forking is checked. If forking takes place, two symmetrical channels are formed at fork point. Then, channel time is revised with the elimination of the lowest energy.

xii. After updating all values in the population, the procedure continues to the next iteration and the processes are repeated until the maximum iteration is reached.

xiii. The optimal number of input delays, feedback delays, and hidden layer neurons are sent to the NARXNN for final training and validation. The flowchart of LSA is presented in Fig. 5.

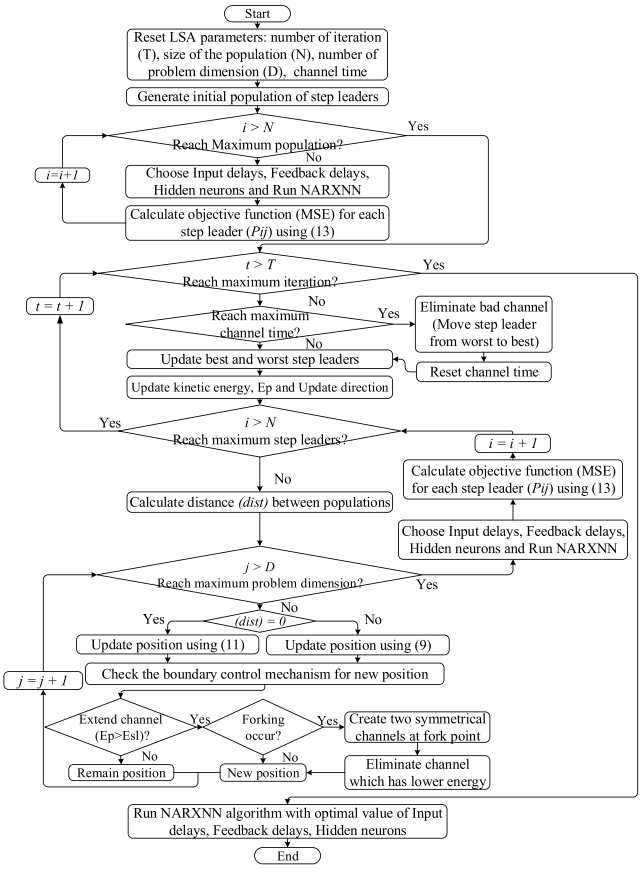

FIGURE 5. Flowchart of LSA.

C. MODEL EVALUATION

Finally, the proposed model is trained and validated by training and testing data with the optimal value of input delays, feedback delays, and hidden layer neurons. Different statistical error terms are used to verify the performance of the proposed model. The training process starts using optimal values achieved from LSA algorithm. The SOC is estimated and compared with the reference value. The reference value is obtained from coulomb counting method with an adjustable current sensor. The performance of the proposed model is checked based on root means square error (RMSE), mean absolute error (MAE) and mean absolute percentage error (MAPE). The mathematical equations of these statistical errors are expressed as follows:

$$RMSE = \sqrt{\frac{1}{N}\sum_{i=1}^{N}(I_{es} - I_a)^2} \tag{15}$$

$$MAE = \frac{1}{N}\sum_{i=1}^{N}(I_{es} - I_a) \tag{16}$$

$$MAPE = \frac{1}{N}\sum_{i=1}^{N}\left|\frac{I_a - I_{es}}{I_a}\right| \tag{17}$$

V. RESULTS AND DISCUSSION

A. OBJECTIVE FUNCTION PERFORMANCE

Generally, optimization is a method of searching the best solutions to problems after determining the objective function

subjected to constraints. An objective function is important for the optimization method in order to obtain a minimum error. Optimal design, optimal management, optimal parameters of a controller, minimal cost and minimal error, could be used as an objective function, depending on the certain application. In this research, mean absolute error (MSE) is selected as the objective function. The results are compared to NARXNN based PSO algorithm using same iterations and population size. The objective function of LSA is assessed in order to find the lowest MSE of LSA and PSO in FUDS and US06 cycles at different temperatures. In FUDS cycle, the minimum value of the MSE of 4.9×10^{-5}, 1.6×10^{-5} and 1.4×10^{-5} are achieved after 45, 10 and 46 iterations in NARXNN based PSO model, whereas in NARXNN based LSA model, MSE value reaches 4.6×10^{-5}, 1.3×10^{-5} and 1.25×10^{-5} after 35, 19 and 71 iterations at 0°C, 25°C and 45°C respectively. In the US06 cycle, NARXNN based PSO model obtains MSE of 4.5×10^{-5}, 3.7×10^{-5} and 1.37×10^{-5} after 14, 62 and 43 iterations at 0°C, 25°C and 45°C, respectively. However, the value of the objective function is lower in NARXNN based LSA model than NARXNN based PSO model achieving MSE of 3.8×10^{-5}, 1.7×10^{-5} and 1.1×10^{-5} after 35, 32 and 72 iterations at 0°C, 25°C and 45°C, respectively. The convergence characteristics curves of FUDS and US06 are presented in Fig. 6. In both drive cycles, LSA delivers better results than PSO in terms obtaining the lowest MSE which proves high accuracy. It is also observed that MSE declines as the temperature increases. SOC varies with the change in temperature. The ambient temperature acceleration causes an increase in battery capacity. The temperature rise increases the activity of the electrolyte and decreases the viscosity which causes ion diffusion [32].

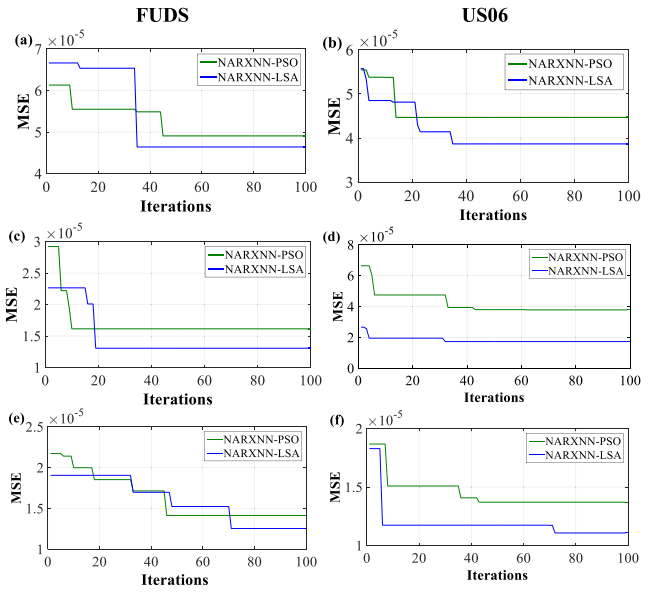

FIGURE 6. Convergence characteristics curves of (a-b) 0°C, (c-d) 25° and, (e-f) 45°C.

B. OPTIMAL PARAMETERS

Table 1 and 2 present the optimal parameters of NARXNN model obtained from FUDS and US06 cycles. In FUDS cycle, the NARXNN based PSO algorithm attains inputs delays of 5, 4, 5 and feedback delays of 5, 2, 3 and hidden neurons of 12, 19, 18 after 45, 10 and 46 iterations at 0°C, 25°C, and 45°C, respectively. Likewise, in NARXNN based LSA model, the optimal numbers of input delays, feedback delays, and hidden layer neurons are computed to be 7,3,3; 6,2,3; 9,16,11 at 0°C, 25°C, and 45°C, respectively after 35, 19 and 71 iterations.

TABLE 1. Optimal parameter in FUDS cycle.

Model	NARXNN-PSO			NARXNN-LSA		
Temperatures	0°C	25°C	45°C	0°C	25°C	45°C
Input Delays	5	4	5	7	3	3
Feedback Delays	5	2	3	6	2	3
Hidden layer neurons	12	19	18	9	16	11

TABLE 2. Optimal parameter in US06 cycle.

Model	NARXNN-PSO			NARXNN-LSA		
Temperatures	0°C	25°C	45°C	0°C	25°C	45°C
Input Delays	8	3	8	4	5	5
Feedback Delays	2	3	3	7	8	5
Hidden layer neurons	6	5	11	18	17	15

In US06 cycle, NARXNN-PSO model achieves optimal value of input delays, feedback delays and hidden neurons of 8,3,8; 2,3,3; 6,5,11 after 14, 62 and 43 iterations at 0°C, 25°C and 45°C, respectively whereas NARXNN-LSA model obtains the best optimization results estimating optimal value of input delays, feedback delays and hidden neurons of 4,5,5; 7,8,5; 18,17,15 after 35, 32 and 72 iterations at 0°C, 25°C and 45°C, respectively.

C. TRAINING PERFORMANCE

The proposed recurrent NARXNN has the improved SOC learning and fast training performance since it converges at 8, 7 and 10 epochs at 0°C, 25°C, and 45°C respectively in FUDS cycle. On the contrary, the best validation performance is achieved at 24, 20 and 6 epochs at 0°C, 25°C, and 45°C respectively, in the US06 cycle. The SOC training and validation performance of recurrent NARXNN for SOC estimation are presented in Fig.7.

D. SOC ESTIMATION

SOC is estimated using NARXNN algorithm based on LSA in FUDS and US06 cycles, respectively as shown in Fig. 8 and Fig. 9. To evaluate the superiority of LSA, a comparative analysis between NARXNN based LSA and NARXNN based PSO is performed at 0°C, 25°C and 45°C, respectively. The red line indicates the SOC estimated by coulomb counting method whereas the lines highlighted in green and blue indicate the SOC estimated by NARXNN based PSO and NARXNN based LSA, respectively. Since current sensor was carefully adjusted, therefore, SOC estimated by coulomb

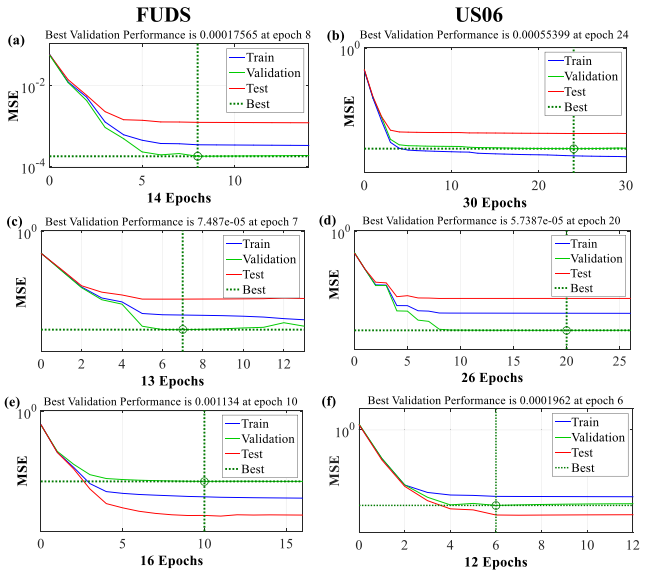

FIGURE 7. SOC training performance using NARX neural network' (a-b) 0°C, (c-d) 25° and, (e-f) 45° C.

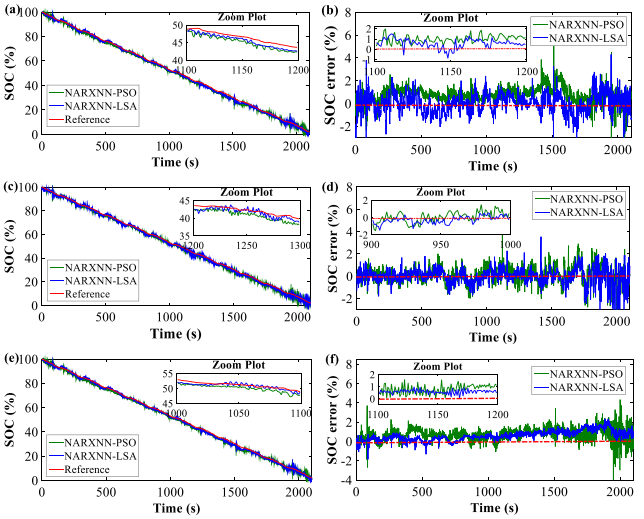

FIGURE 9. Estimation results in US06 cycle (a) SOC at 0°C (b) SOC error at 0°C (c) SOC at 25°C (d) SOC error at 25°C (e) SOC at 45°C (f) SOC error at 45°C.

counting method is regarded as a true SOC and named as a reference. It is observed that the estimation curves simulated by the NARXNN based PSO have more fluctuations than that of NARXNN based LSA algorithm which proves that NARXNN based LSA model has high accuracy and strong robustness.

Fig. 8 and Fig. 9 also present the absolute error which is found by subtracting the actual SOC from the estimated SOC. In NARXNN based PSO model, the error bound is found at [−10.9% ∼7.6%], [−1.7% ∼4.3%], [−4% ∼3.1%] for FUDS cycle with high oscillations and some high peaks at certain intervals at 0°C, 25°C, and 45°C, respectively. Nevertheless, in NARXNN based LSA model, absolute error is more stable and has less fluctuation where the error bound lies

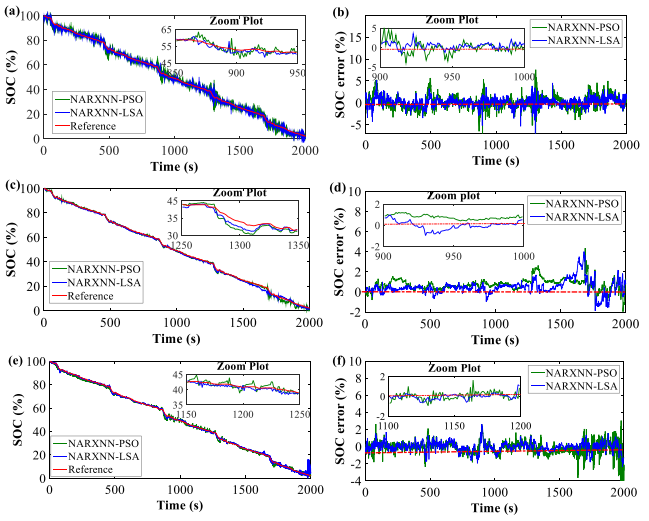

FIGURE 8. Estimation results in FUDS cycle (a) SOC at 0° C (b) SOC error at 0°C (c) SOC at 25°C (d) SOC error at 25°C (e) SOC at 45°C (f) SOC error at 45°C.

at [−8.5% ∼4.8%], [−1.4% ∼4%], [−2.3% ∼2.6%] at 0°C, 25°C, and 45°C, respectively. Similarly, in the US06 cycle, NARXNN based LSA model has less randomness than that of NARXNN based PSO model having an absolute error of [−5.6% ∼4.3%], [−4.6% ∼3.5%], [−1.8% ∼2.9%] at 0°C, 25°C, and 45°C respectively. The simulation results demonstrate that the performance of NARXNN based LSA method has higher robustness and less estimation error compared to that of NARXNN based PSO method at different temperature conditions.

In this research, we investigated the individual lithium-ion cell characteristics to monitor SOC which was considered as the average SOC of the battery pack. However, overcharge and over discharge of lithium-ion battery may occur which results in cell inconsistency problem. We have already developed charge equalization controller (CEC) model towards monitoring and balancing the voltage level of lithium-ion battery pack [33]–[35]. The developed system has achieved excellent results in terms of simplicity in design, control and execution, equalization speed and efficiency with low power loss. We used OCV method to monitor SOC in each cell of the battery pack. However, OCV method has the shortcoming of taking a long duration to reach a balanced state. Therefore, the obtained accurate SOC estimation results using NARXNN with LSA model could be used for implementing CEC to address cell inconsistency in lithium-ion battery packs.

E. PERFORMANCE COMPARISON

To assess the dominance of NARXNN-LSA model, a comprehensive performance analysis of proposed algorithm and BPNN-LSA, RBFNN-LSA models is investigated. The performance comparison of three optimal models is analyzed using FUDS and US06 cycles, as shown in Fig. 10 and Fig. 11, respectively. Similar to NARXNN-LSA model,

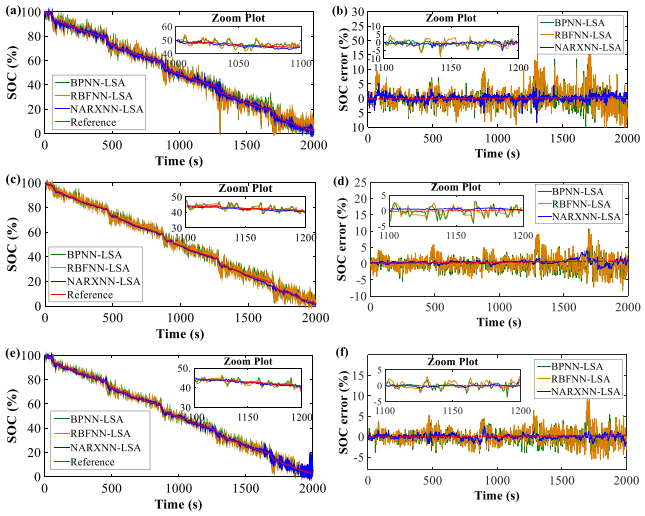

FIGURE 10. Comparison among BPNN-LSA, RBFNN-LSA and NARXNN-LSA models in FUDS cycle (a) SOC at 0°C (b) SOC error at 0°C (c) SOC at 25°C (d) SOC error at 25°C (e) SOC at 45°C (f) SOC error at 45°C.

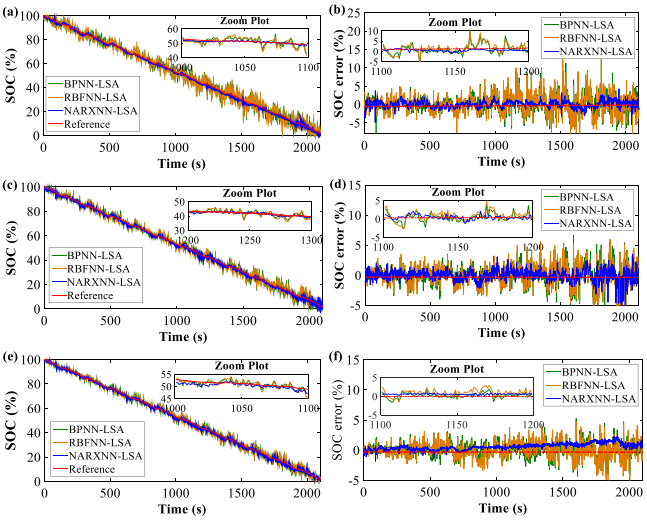

FIGURE 11. Comparison among BPNN-LSA, RBFNN-LSA and NARXNN-LSA models in US06 cycle (a) SOC at 0°C (b) SOC error at 0°C (c) SOC at 25°C (d) SOC error at 25°C (e) SOC at 45°C (f) SOC error at 45°C.

the hyperparameters of BPNN and RBFNN including hidden neurons, learning rate, and spread value are tuned using LSA.

The simulation of three optimal models is performed using similar inputs, data division, training algorithm, activation function, population, and iterations. It is clearly noticed from Fig. 10 and Fig. 11 that, SOC estimated by NARXNN based LSA algorithm is very much aligned with the reference value and has less SOC error compared to BPNN based LSA and RBFNN based LSA models at different temperature effects. BPNN based LSA and RBFNN based LSA diverges in higher extent from the actual SOC whereas NARXNN based LSA delivers better quality output and has stable SOC error with few fluctuations. The results validate that the proposed model achieves satisfactory performance in estimating SOC with high accuracy.

TABLE 3. Performance comparison in FUDS drive cycle.

Model	Temperature	RMSE (%)	MAE (%)	MAPE (%)	SOC Error (%)
BPNN-LSA	0°C	2.63	1.77	13.82	[-10.8, 13.7]
	25°C	1.82	1.26	11.78	[-6.9, 10.7]
	45°C	1.43	0.98	8.75	[-4.8, 9.2]
RBFNN-LSA	0°C	3.67	2.64	21.47	[-11.6, 19.2]
	25°C	2.26	1.71	19.32	[-8.5, 10.4]
	45°C	1.79	1.26	13.12	[-5.3, 9.3]
NARXNN-LSA	0°C	1.26	0.76	10.59	[-8.5, 4.8]
	25°C	0.68	0.48	6.45	[-1.4, 4]
	45°C	0.52	0.34	5.28	[-2.3, 2.6]

TABLE 4. Performance comparison in US06 drive cycle.

Model	Temperature	RMSE (%)	MAE (%)	MAPE (%)	SOC Error (%)
BPNN-LSA	0°C	2.17	1.52	13.07	[-10.41,12.2]
	25°C	1.43	1.03	10.76	[-6.1, 6.6]
	45°C	1.09	0.78	6.48	[-5.1, 4.4]
RBFNN-LSA	0°C	2.62	1.89	16.72	[-9.6 , 15.3]
	25°C	1.67	1.26	15.75	[-6.8 , 5.9]
	45°C	1.33	1.01	8.78	[-5.8, 4.7]
NARXNN-LSA	0°C	0.89	0.82	8.91	[-5.6 , 4.3]
	25°C	0.62	0.53	4.24	[-4.6 , 3.5]
	45°C	0.55	0.43	3.38	[-1.8 , 2.9]

TABLE 5. Computational time comparison in two drive cycle.

Model	Temperature	Computational time (s)	
		FUDS	US06
BPNN-LSA	0°C	65.49	68.18
	25°C	62.16	65.58
	45°C	58.57	62.73
RBFNN-LSA	0°C	42.19	43.08
	25°C	39.58	41.37
	45°C	38.25	40.41
NARXNN-LSA	0°C	8.59	10.12
	25°C	7.75	9.42
	45°C	7.41	8.38

Table 3 shows the evaluation results of three models based on RMSE, MAE, MAPE and SOC error in FUDS cycle. It is observed that the temperature has a significant influence on battery performance as the high temperatures result in a low error and high accuracy. The RMSE for the NARXNN-LSA model is computed as 0.68% at 25°C which is a 63% and 70% decrease from the BPNN-LSA and RBFNN-LSA model, respectively. Furthermore, the proposed model has higher RMSE of 1.26% and lower RMSE of 0.52% than the value obtained at 25°C which is a 52%, 66% reduction at 0°C and 64%, 71% reduction at 45°C, from the BPNN-LSA and RBFNN-LSA models, respectively.

Similar kind of results is also achieved while estimating MAE. The MAE value of the NARXNN-LSA model is dropped by 57% and 71% at 0°C compared to BPNN-LSA and RBFNN-LSA models, respectively. As the temperature increases, the value of MAE is reduced in NARXNN-LSA model and reaches 0.48% and 0.34% at 25°C and 45°C, respectively. There is an also an improvement of MAE in the proposed model where the error is decreased by 62%, 72% at 25°C and 65%, 73%, at 45°C, in comparison to the

TABLE 6. Comparison of proposed SOC estimation method with The existing methods.

Method	Test battery	Test Profile	Temperature	Error
ANN + UKF [19]	2.3 Ah $LiFePO_4$	(i) US06 (ii) FUDS	0°C to 50°C	RMSE 0.9%~2.5% in US06 RMSE 0.5%~2.2% in FUDS
ELM + Adaptive UKF [39]	2.6 Ah Samsung lithium-ion cell	0.52 A 50% duty cycle pulse discharge	25°C (ambient)	Maximum error <1.5%
Adaptive UKF + SVM [40]	70 Ah Kokam lithium polymer battery	Two discharge current profiles (i) -224 A to 396 A (ii) -110 A to 430 discharge duration 1108 seconds	25°C to 42°C	MAE < 2%
Fuzzy neural network + genetic algorithm [41]	10Ah MRL/ITRI lithium-ion batteries	Constant resistance discharge (13 A)	25°C (ambient)	Average percentage error (APE) < 0.9%
BPNN+ BSA [37]	2 Ah 18650 $LiNiMnCoO_2$/NMC	(i) FUDS (ii) Dynamic Stress Test (DST)	0°C, 25°C and 45°C	RMSE 0.57%~1.74% in FUDS MAE 0.38%~0.87% in FUDS RMSE 0.48% ~1.47% in DST MAE 0.32%~0.76% in DST
RBFNN [21]	6 Ah $LiMn_2O_4$	(i) Urban Dynamometer Driving Schedule (UDDS) (ii) Economic Commission of Europe (ECE)	0°C, 25°C, and 40°C	MAE < 5% under different temperatures and aging cycles
RNN + LSTM [38]	2.9 Ah Panasonic $LiNiCoAlO_2$/ NCA	Dynamic drive cycles, ±18 A,	0°C, 10°C and 25°C	RMSE 1.11% ~2.44% MAE 0.77%~2.08%
Recurrent NARXNN + LSA (proposed in this paper)	2 Ah 18650 $LiNiMnCoO_2$/NMC	(i) FUDS (ii) US06	0°C, 25°C and 45°C	RMSE 0.52% ~1.26% in FUDS MAE 0.34%~0.76% in FUDS RMSE 0.55%~0.89% in US06 MAE 0.43%~0.82% in US06

BPNN-LSA and RBFNN-LSA models, respectively. In addition, there is a decrease in MAPE of the proposed method where the error is reduced by 45%, 67%, compared to BPNN-LSA and RBFNN-LSA models, respectively at 25°C.

The comparison results are also verified using US06 cycle, as presented in Table 4. The RMSE in NARXNN-LSA is estimated to be 0.62% at 25°C whereas the BPNN-LSA and RBFNN-LSA methods have RMSE of 1.43%, 1.67%, respectively which is a 131%, 169% increase from the proposed method. Besides, there is a reduction in MAE of the proposed model which is dropped by 49%, 58%, respectively compared to other two models, at 25°C. The value of MAPE is also improved in proposed model and decreased by 61% and 73%, respectively, compared to other two models, at 25°C. Moreover, the proposed method achieves very narrow SOC error compared to other two neural network models in both drive cycles. It is also observed that BPNN-LSA model has a lower computational error than that of RBFNN-LSA model. However, BPNN-LSA model needs more time for weight, bias training, and updating. In both drive cycles, NARXNN-LSA model outperforms the other two ANN models.

BPNN-LSA and RBFNN-LSA models also fall short while estimating SOC with high speed. The computational time is defined as the duration it requires for the complete training and testing to estimate SOC. As expected, that the NARXNN-LSA model is also dominant to the BPNN-LSA and RBFNN-LSA models in achieving SOC with short duration, as shown in Table 5. For instance, in FUDS cycle, BPNN-LSA and RBFNN-LSA model takes 62.16 seconds and 39.58 seconds, respectively for SOC estimation at 25°C; however, NARXNN-LSA model training and evaluation are executed in only 7.75 seconds. The similar type of outcomes is also found in the US06 cycle. A substantially higher number of epochs is required in BPNN-LSA and RBFNN-LSA models than NARXNN-LSA model to converge the estimated value to the real value which demonstrates that the NARXNN-LSA model decreases computational load and thus increases the estimation speed. In summary, recurrent NARXNN with LSA optimization technique has demonstrated to be a most efficient model and provides the best performance in terms of high accuracy, strong robustness and quick computational speed under different EV profiles and temperatures.

F. COMPARITIVE VALIDATION WITH THE EXISTING METHODS

To further evaluate the performance of the developed model, Table 6 shows the comparison of error between the existing SOC estimation methods and proposed method. A total of seven case studies including unscented Kalman filter (UKF), SVM, extreme learning machine (ELM), fuzzy logic, genetic algorithm, backtracking search algorithm (BSA), long-short term memory (LSTM) and different ANN techniques are considered in this comparison. NARXNN with LSA shows superiority and robustness when compared with the existing SOC estimation techniques. For example, our previous research based on BPNN with BSA [36] model estimated RMSE of 0.57%∼1.74% and MAE of 0.38%∼0.87% in FUDS cycle at varying temperatures conditions. However, the proposed NARXNN-LSA improves the SOC estimation results and obtains RMSE of 0.52%∼1.26% and MAE of 0.34%∼0.76%. Moreover, the proposed model outperforms

RNN based LSTM [37] model and ANN based UKF [19] model at different load profiles and temperatures conditions.

VI. CONCLUSION

This paper presents an enhanced recurrent NARXNN based LSA model for the improvement of SOC estimation performance. The study has chosen lithium-ion battery because of high capacity and longevity. The input delay, feedback delay and hidden neurons of the NARXNN architecture are the most important parameters. Nonetheless, these parameters are normally assigned randomly or by experience, which do not provide the satisfactory solution. Hence, LSA is used to improve the NARXNN model ability by finding the global optimal solution. The overall contributions of the established model are the strong robustness and efficient SOC estimation under different dynamic load profiles and temperatures effects. The main innovative points of this research are highlighted as follows: (1) The computation intelligent of NARX algorithm is improved with the implementation of LSA, (2) the proposed NARXNN based LSA algorithm works efficiently without considering battery model and complex mathematical equations, (3) the efficiency of LSA is checked with PSO where LSA is dominant to PSO in term of achieving the lowest objective function, (4) the performance of the proposed NARXNN- model is verified under different discharge current profiles and temperatures. The developed model offers high robustness and accuracy having SOC error of [−1.4%∼4%] and [−4.6%∼3.5%] in FUDS and US06 cycle respectively, at 25°C, (5) the effectiveness of NARXNN-LSA algorithm is evaluated by comparing with BPNN-LSA and RBFNN-LSA algorithm in which NARXNN-LSA outperforms other two algorithms, (6) the developed model has high estimation speed compared to other neural network methods. Finally, the NARXNN based LSA model can be considered a good balance between complexity and desired accuracy while saving time and human energy by avoiding the ineffective time-consuming techniques employed by other approaches. Comprehensive experimental results would verify the accuracy, adaptability, and superiority of NARXNN-LSA model. The proposed model could be designed in the prototype hardware implementation in modularized design for the real-time EV applications.

REFERENCES

[1] Environmental Protection Agency. *Global Greenhouse Gas Emissions Data, Greenhouse Gas (GHG) Emissions*. Accessed: Jan. 4, 2018. [Online]. Available: https://www.epa.gov/ghgemissions/global-greenhouse-gas-emissions-data

[2] M. A. Hannan, M. S. H. Lipu, A. Hussain, and A. Mohamed, "A review of lithium-ion battery state of charge estimation and management system in electric vehicle applications: Challenges and recommendations," *Renew. Sustain. Energy Rev.*, vol. 78, pp. 834–854, Oct. 2017.

[3] D. Anseán, M. González, V. M. García, J. C. Viera, J. C. Antón, and C. Blanco, "Evaluation of $LiFePO_4$ batteries for electric vehicle applications," *IEEE Trans. Ind. Appl.*, vol. 51, no. 2, pp. 1855–1863, Mar./Apr. 2015.

[4] M. Cacciato, G. Nobile, G. Scarcella, and G. Scelba, "Real-time model-based estimation of SOC and SOH for energy storage systems," *IEEE Trans. Power Electron.*, vol. 32, no. 1, pp. 794–803, Jan. 2017.

[5] R. Xiong, J. Cao, Q. Yu, H. He, and F. Sun, "Critical review on the battery state of charge estimation methods for electric vehicles," *IEEE Access*, vol. 6, pp. 1832–1843, 2017.

[6] L. Liu, L. Y. Wang, Z. Chen, C. Wang, F. Lin, and H. Wang, "Integrated system identification and state-of-charge estimation of battery systems," *IEEE Trans. Energy Convers.*, vol. 28, no. 1, pp. 12–23, Mar. 2013.

[7] M. S. H. Lipu, M. A. Hannan, A. Hussain, and M. H. M. Saad, "Optimal BP neural network algorithm for state of charge estimation of lithium-ion battery using PSO with PCA feature selection," *J. Renew. Sustain. Energy*, vol. 9, no. 6, p. 64102, Nov. 2017.

[8] K. S. Ng, C.-S. Moo, Y.-P. Chen, and Y.-C. Hsieh, "Enhanced coulomb counting method for estimating state-of-charge and state-of-health of lithium-ion batteries," *Appl. Energy*, vol. 86, no. 9, pp. 1506–1511, Sep. 2009.

[9] M. Coleman, C. K. Lee, C. Zhu, and W. G. Hurley, "State-of-charge determination from EMF voltage estimation: Using impedance, terminal voltage, and current for lead-acid and lithium-ion batteries," *IEEE Trans. Ind. Electron.*, vol. 54, no. 5, pp. 2550–2557, Oct. 2007.

[10] K.-T. Lee, M.-J. Dai, and C.-C. Chuang, "Temperature-compensated model for lithium-ion polymer batteries with extended Kalman filter state-of-charge estimation for an implantable charger," *IEEE Trans. Ind. Electron.*, vol. 65, no. 1, pp. 589–596, Jan. 2018.

[11] R. Xiong, Y. Zhang, H. He, X. Zhou, and M. Pecht, "A double-scale, particle-filtering, energy state prediction algorithm for lithium-ion batteries," *IEEE Trans. Ind. Electron.*, vol. 65, no. 2, pp. 1526–1538, Feb. 2018.

[12] S. Muhammad, M. U. Rafique, S. Li, Z. Shao, Q. Wang, and N. Guan, "A robust algorithm for state-of-charge estimation with gain optimization," *IEEE Trans. Ind. Informat.*, vol. 13, no. 6, pp. 2983–2994, Dec. 2017.

[13] W. Li, L. Liang, W. Liu, and X. Wu, "State of charge estimation of lithium-ion batteries using a discrete-time nonlinear observer," *IEEE Trans. Ind. Electron.*, vol. 64, no. 11, pp. 8557–8565, Nov. 2017.

[14] I.-S. Kim, "The novel state of charge estimation method for lithium battery using sliding mode observer," *J. Power Sour.*, vol. 163, no. 1, pp. 584–590, 2006.

[15] G.-C. Hsieh, L.-R. Chen, and K.-S. Huang, "Fuzzy-controlled Li-ion battery charge system with active state-of-charge controller," *IEEE Trans. Ind. Electron.*, vol. 48, no. 3, pp. 585–593, Jun. 2001.

[16] J. C. Á. Antón, P. J. G. Nieto, C. B. Viejo, and J. A. V. Vilán, "Support vector machines used to estimate the battery state of charge," *IEEE Trans. Power Electron.*, vol. 28, no. 12, pp. 5919–5926, Dec. 2013.

[17] L. Jin, S. Li, B. Hu, M. Liu, and J. Yu, "Noise-suppressing neural algorithm for solving time-varying system of linear equations: A control-based approach," *IEEE Trans. Ind. Informat.*, Jan. 2018, doi: 10.1109/TII.2018.2798642.

[18] Y. Shen, "Adaptive online state-of-charge determination based on neuro-controller and neural network," *Energy Convers. Manage.*, vol. 51, no. 5, pp. 1093–1098, 2010.

[19] W. He, N. Williard, C. Chen, and M. Pecht, "State of charge estimation for Li-ion batteries using neural network modeling and unscented Kalman filter-based error cancellation," *Int. J. Elect. Power Energy Syst.*, vol. 62, pp. 783–791, Nov. 2014.

[20] M. Charkhgard and M. Farrokhi, "State-of-charge estimation for lithium-ion batteries using neural networks and EKF," *IEEE Trans. Ind. Electron.*, vol. 57, no. 12, pp. 4178–4187, Dec. 2010.

[21] L. Kang, X. Zhao, and J. Ma, "A new neural network model for the state-of-charge estimation in the battery degradation process," *Appl. Energy*, vol. 121, pp. 20–27, May 2014.

[22] H. Chaoui and C. C. Ibe-Ekeocha, "State of charge and state of health estimation for lithium batteries using recurrent neural networks," *IEEE Trans. Veh. Technol.*, vol. 66, no. 10, pp. 8773–8783, Oct. 2017.

[23] H. Shareef, A. A. Ibrahim, and A. H. Mutlag, "Lightning search algorithm," *Appl. Soft Comput.*, vol. 36, pp. 315–333, Nov. 2015.

[24] L. Jin, S. Li, and B. Hu, "RNN models for dynamic matrix inversion: A control-theoretical perspective," *IEEE Trans. Ind. Informat.*, vol. 14, no. 1, pp. 189–199, Jan. 2018.

[25] T.-N. Lin, C. L. Giles, B. G. Horne, and S.-Y. Kung, "A delay damage model selection algorithm for NARX neural networks," *IEEE Trans. Signal Process.*, vol. 45, no. 11, pp. 2719–2730, Nov. 1997.

[26] J. M. P. Menezes, Jr., and G. A. Barreto, "Long-term time series prediction with the NARX network: An empirical evaluation," *Neurocomputing*, vol. 71, nos. 16–18, pp. 3335–3343, Oct. 2008.

[27] D. Argyropoulos, D. S. Paraforos, R. Alex, H. W. Griepentrog, and J. Müller, "NARX neural network modelling of mushroom dynamic vapour sorption kinetics," *IFAC-PapersOnLine*, vol. 49, no. 16, pp. 305–310, 2016.
[28] H. Wang and G. Song, "Innovative NARX recurrent neural network model for ultra-thin shape memory alloy wire," *Neurocomputing*, vol. 134, pp. 289–295, Jun. 2014.
[29] F. Zheng, Y. Xing, J. Jiang, B. Sun, J. Kim, and M. Pecht, "Influence of different open circuit voltage tests on state of charge online estimation for lithium-ion batteries," *Appl. Energy*, vol. 183, pp. 513–525, Dec. 2016.
[30] M. S. H. Lipu, M. A. Hannan, and A. Hussain, "Feature selection and optimal neural network algorithm for the state of charge estimation of lithium-ion battery for electric vehicle application," *Int. J. Renew. Energy Res.*, vol. 7, no. 4, pp. 1700–1708, Dec. 2017.
[31] *CALCE, Lithium-Ion Battery Experimental Data*. Accessed: Jan. 5, 2017. [Online]. Available: http://www.calce.umd.edu/batteries/data.htm
[32] D. H. Doughty, E. P. Roth, C. C. Crafts, G. Nagasubramanian, G. Henriksen, and K. Amine, "Effects of additives on thermal stability of Li ion cells," *J. Power Sources*, vol. 146, nos. 1–2, pp. 116–120, 2005.
[33] M. A. Hannan, M. M. Hoque, P. J. Ker, R. A. Begum, and A. Mohamed, "Charge equalization controller algorithm for series-connected lithium-ion battery storage systems: Modeling and applications," *Energies*, vol. 10, no. 9, p. 1390, 2017.
[34] M. A. Hannan, M. M. Hoque, S. E. Peng, and M. N. Uddin, "Lithium-ion battery charge equalization algorithm for electric vehicle applications," *IEEE Trans. Ind. Appl.*, vol. 53, no. 3, pp. 2541–2549, May/Jun. 2017.
[35] M. M. Hoque, M. A. Hannan, and A. Mohamed, "Optimal algorithms for the charge equalisation controller of series connected lithium-ion battery cells in electric vehicle applications," *IET Elect. Syst. Transp.*, vol. 7, no. 4, pp. 267–277, Dec. 2017.
[36] M. A. Hannan, M. S. H. Lipu, A. Hussain, M. H. Saad, and A. Ayob, "Neural network approach for estimating state of charge of lithium-ion battery using backtracking search algorithm," *IEEE Access*, vol. 6, pp. 10069–10079, 2018.
[37] E. Chemali, P. Kollmeyer, M. Preindl, R. Ahmed, and A. Emadi, "Long short-term memory networks for accurate state-of-charge estimation of Li-ion batteries," *IEEE Trans. Ind. Electron.*, vol. 65, no. 8, pp. 6730–6739, Aug. 2018.
[38] J. Du, Z. Liu, and Y. Wang, "State of charge estimation for Li-ion battery based on model from extreme learning machine," *Control Eng. Pract.*, vol. 26, pp. 11–19, May 2014.
[39] J. Meng, G. Luo, and F. Gao, "Lithium polymer battery state-of-charge estimation based on adaptive unscented Kalman filter and support vector machine," *IEEE Trans. Power Electron.*, vol. 31, no. 3, pp. 2226–2238, Mar. 2016.
[40] Y.-S. Lee, W.-Y. Wang, and T.-Y. Kuo, "Soft computing for battery state-of-charge (BSOC) estimation in battery string systems," *IEEE Trans. Ind. Electron.*, vol. 55, no. 1, pp. 229–239, Jan. 2008.

MOLLA S. HOSSAIN LIPU received the B.S. degree in electrical and electronic engineering from the Islamic University of Technology, Gazipur, Bangladesh, in 2008, and the M.S. degree in energy from the Asian Institute of Technology, Bangkok, Thailand, in 2013. He is currently pursuing the Ph.D. degree with the Centre for Integrated Systems Engineering and Advanced Technologies, Faculty of Engineering and Built Environment, Universiti Kebangsaan Malaysia, Bangi, Malaysia. He is currently an Assistant Professor of electrical and electronic engineering with the University of Asia Pacific, Dhaka, Bangladesh. His research interest includes energy storage systems, artificial intelligence, model optimization, and hybrid renewable energy system.

MAHAMMAD A. HANNAN (M'10–SM'17) received the B.Sc. degree in electrical and electronic engineering from the Chittagong University of Engineering and Technology, Chittagong, Bangladesh, in 1990, and the M.Sc. and Ph.D. degrees in electrical, electronic, and systems engineering from Universiti Kebangsaan Malaysia, Bangi, Malaysia, in 2003 and 2007, respectively. He is currently a Professor of intelligent systems with the Department of Electrical Power Engineering, College of Engineering, Universiti Tenaga Nasional, Malaysia. His research interests include intelligent controllers, power electronics, hybrid vehicles, energy storage systems, image and signal processing, and artificial intelligence. He received numbers of gold awards for his innovative research in ITEX, MTE, INNOFEST, SIIF, and PERINTIS. He is an Associate Editor of the IEEE Access.

AINI HUSSAIN (M'98) received the B.Sc. degree in electrical engineering from Louisiana State University, USA, the M.Sc. degree from UMIST, U.K., and the Ph.D. degree from Universiti Kebangsaan Malaysia. She is currently a Professor with the Centre for Integrated Systems Engineering and Advanced Technologies, Faculty of Engineering and Built Environment, Universiti Kebangsaan Malaysia. Her research interests include decision support systems, machine learning, pattern precognition, signal, and image processing.

MOHAMAD H. M. SAAD received the B.Sc. degree in mechanical and materials engineering and the Ph.D. degree from Universiti Kebangsaan Malaysia in 2017. He is currently a Senior Lecturer with the Department of Mechanical and Materials Engineering, Faculty of Engineering and Built Environment, Universiti Kebangsaan Malaysia. His research interests include artificial intelligence, intelligent systems, and complex event processing.

AFIDA AYOB received the B.Sc. degree in electrical and electronic engineering from The University of Manchester in 2000 and the Ph.D. degree from Newcastle University in 2012. She is currently a Senior Lecturer with the Centre for Integrated Systems Engineering and Advanced Technologies, Faculty of Engineering and Built Environment, Universiti Kebangsaan Malaysia. Her research interests include power electronic, energy storage, and artificial intelligence.

FREDE BLAABJERG (S'86–M'88–SM'97–F'03) received the Ph.D. degree in power electronics from Aalborg University, Aalborg, Denmark. He was with ABB-Scandia, Randers, Denmark, from 1987 to 1988. He is currently a Professor with Aalborg University, Denmark. His current research interests include power electronics and its applications, such as in wind turbines, PV systems, reliability, harmonics, and adjustable speed drives. He received the 18 IEEE Prize Paper Awards, the IEEE PELS Distinguished Service Award in 2009, the EPE-PEMC Council Award in 2010, the IEEE William E. Newell Power Electronics Award in 2014, and the Villum Kann Rasmussen Research Award in 2014. He was the Editor-in-Chief of the IEEE Transactions on Power Electronics from 2006 to 2012. He is nominated in 2014, 2015, and 2016 by Thomson Reuters to be between the most 250 cited researchers in Engineering in the world.